Received: 15 November 2024 | Revised: 18 April 2025 | Accepted: 22 April 2025

DOI: 10.1111/jace.20619

Journal of the American Ceramic Society

RESEARCH ARTICLE

Structural modulation, oriented growth of rock salt, and spinel in (Co(Cr/Mg)FeMnNi) multicomponent oxide and derivatives

Saptarshi Mukherjee | **N. K. Mukhopadhyay** | **Joysurya Basu**

Department of Metallurgical Engineering, Indian Institute of Technology (BHU), Varanasi, India

Correspondence
Joysurya Basu, Department of Metallurgical Engineering, Indian Institute of Technology (BHU), Varanasi 221005, India.
Email: jbasu.met@iitbhu.ac.in

Funding information
Department of Science & Technology, Government of India, Grant/Award Number: TPN-32537

Abstract

Phases, interfaces, microstructure, and stabilization mechanism in multicomponent (Co(Cr/Mg)FeMnNi)-oxide along with its binary, ternary, and quaternary derivatives, synthesized through solid-state route, have been studied by X-ray diffraction and transmission electron microscopy. Formation of single-phase spinel in multicomponent (CoFeMgMnNi)-oxide after sintering at 1473 K for 10 h is being reported with preferential growth of rock salt phase upon longer holding time. Oriented growth of spinel with rock salt and formation of coherent/semi-coherent interface structure helps in minimizing the interface strain. Equimolar ternary derivative, (CoMgNi)-oxide, after sintering at 1473 K for 10 h forms a rock salt phase along with a minor volume fraction of spinel phase. Ternary (CoMgNi)-oxide and multicomponent (CoFeMgMnNi)-oxide, upon prolonged sintering or aging, develop structural modulation with/without chemical partitioning that is evident from the electron diffraction patterns through spot splitting, intensity modulation, and arcing. Single-phase spinel forming (CoCrFeMnNi)-multicomponent oxide develops structurally modulated microstructure upon sintering and quenching, which is being observed for the first time. Stabilization of the multicomponent oxides is explained as a trade-off between the high configurational entropy due to the presence of multiple cations in the cation sublattice and the minimization of strain energy in the crystal of the multicomponent oxide.

KEYWORDS
electron microscopy, high entropy oxide, microstructure, phase stability, rock salt, spinel, strain energy, X-ray diffraction

1 | INTRODUCTION

Spinel and rock salt forming high entropy oxides (HEOs)/multicomponent oxides (MCOs) have garnered tremendous attention in the recent past owing to its favorable properties making it frontrunner candidates for its use in the field of energy conversion, storage, and catalysis.[1–7] Right after the discovery of rock salt HEO in (CoCuMgNiZn)O, less than a decade ago,[8] successful synthesis of phase-pure spinel forming HEO in $(CoCrFeMnNi)_3O_4$ was reported a few years later.[9] Subsequently, a plethora of other HEO forming compositions were reported from each family of ceramic crystal structures.[10,11] A lot of groups have investigated these

two special compositions since then, with primary focus on their functional properties.[12–15] Several substitutions to explore the composition-phase space has also been reported.[16,17] However, phase stability, microstructural evolution, and mechanism behind synergistic effect of entropic stabilization in these HEOs have been comparatively less explored.[18–20] There are a couple of major schools of thought regarding the phase formation and stability of such multicomponent metallic oxides. The overwhelming belief that stabilization of a homogeneous disordered single-phase solid solution stems from the dominance of configurational entropy of mixing in HEOs, sits on one hand.[21,22] On the other hand, enthalpic penalties induced precipitation of related multicomponent secondary phases and/or defect microstructure formation has also been explored by a few research groups.[23–25] However, direct experimental evidences for such deviations are scarce. Additionally, the spinel crystal structure is relatively more complex than rock salt counterpart owing to the greater degrees of freedom of void filling by cations, rendering it amenable to ordering, phase separation, or distortions.[26–31]

The current work has been carried out to understand the stability and phase-pure nature of the original spinel forming HEO. In order to arrive at satisfactory conclusions from previously unreported experimental evidences, it is necessary to accumulate findings from its derivative lower order oxides. It has been found out that equimolar ternary (CoMgNi)-oxide with rock salt structure gives rise to phase-pure spinel structure upon partial substitution by Mn-ions and Fe-ions. This gives rise to $(CoFeMgMnNi)_3O_4$ single-phase spinel forming MCO. However, structural modulation and oriented inter-growth of related phases sharing semi-coherent boundaries in both the above-mentioned equimolar ternary and quinary MCOs could be discerned, which was not envisaged previously. Furthermore, a phase separation event along specific crystallographic directions, although at its nascent stage, is found to influence the microstructural formation in the $(CoCrFeMnNi)_3O_4$ spinel HEO.

2 | MATERIALS AND METHODS

Multicomponent, equimolar oxides of (CoFeMgMnNi), (CoCrFeMnNi), and its binary, ternary, and quaternary derivatives, that is, (MgNi)-oxide, (CoNi)-oxide, (CoMgNi)-oxide, (CoFeMgNi)-oxide, and (CoMgMnNi)-oxide have been synthesized by solid-state synthesis route due to the ease of materials handling and probability of success. Starting precursor oxides, that is, Co(II, III)O, Cr(III)O, Fe(II, III)O, MgO, Mn(III)O, and NiO (>99.8 at% purity) were procured from either Alfa Aesar or Sigma–Aldrich. The main objective of this research has been to investigate the phase stability and microstructural evolution of equimolar quinary (CoCrFeMnNi)-oxide and (CoFeMgMnNi)-oxide. However, the experimental data could not be rationalized on its own, for which several lower order oxides were systematically synthesized and characterized. The oxides in powder form were mixed in stoichiometric proportions for all the binary, ternary, quaternary, and quinary compositions before they were mixed thoroughly in a mortar and pestle. As-mixed equimolar ternary oxide of (CoMgNi) was further ball milled for 40 h in a Retsch PM400 planetary ball mill in dry environment using zirconia vial and balls at 200 rpm with 10:1 ball to powder ratio. It is noted that all the above-mentioned compositions too have been ball milled as proof of concept; however, the particular case study of (CoMgNi) has been elucidated for the purpose of clarity. During ball milling, the milling process was paused for 30 s after every 60 s of milling to avoid dynamic recrystallization. In order to study the phase evolution in the mixed powder, samples were collected after 5, 15, and 40 h of milling. The collected samples were characterized by X-ray diffraction (XRD) in a Rigaku MiniFlex600 table top X-ray diffractometer with Cu-K_α ($\lambda = 1.54$ Å) radiation operated at 40 kV accelerating voltage with 15 mA tube current.

Precursor oxides, mixed in stoichiometric proportions, for all the binary, ternary, quaternary, and quinary compositions were compacted in a uniaxial hydraulic press with 4 T load to produce the green compacted pellets of ~12 mm diameter and ~4–5 mm thickness. The green compacted pellets were sintered at ~1473 K for 10 h in air before they were water quenched. Quinary (CoFeMgMnNi)-oxide was also sintered at 1473 K for 100 h, in addition to the 10 h sintering and it was then water quenched. Additionally, the ternary (CoMgNi)-oxide was further aged at 723 K for 120 h in air and then it was water quenched. Sintering and aging treatments were carried out in a platinum crucible with the lid on. In order to maintain perfect stoichiometry and avoid contamination, a number of pellets with identical composition were stacked together in the platinum crucible and the pellet from the center of the stack was taken for further studies. It is worth mentioning in this context that the use of the terms "stoichiometric" and "equimolar" must be dealt with cautiously. They have been used with respect to the synthesis parameters of the as-mixed powders. It is well understood that sintering/heat treatment may alter the overall stoichiometry and equimolarism; hence, its effect on the phase stability and microstructural evolution has been investigated in detail. Sintered, quenched ternary (CoMgNi)-oxide, sintered, quenched (CoCrFeMnNi)-oxide, and long-sintered, quenched (CoFeMgMnNi)-oxide were characterized by XRD using a Malvern Panalytical high-resolution X-ray

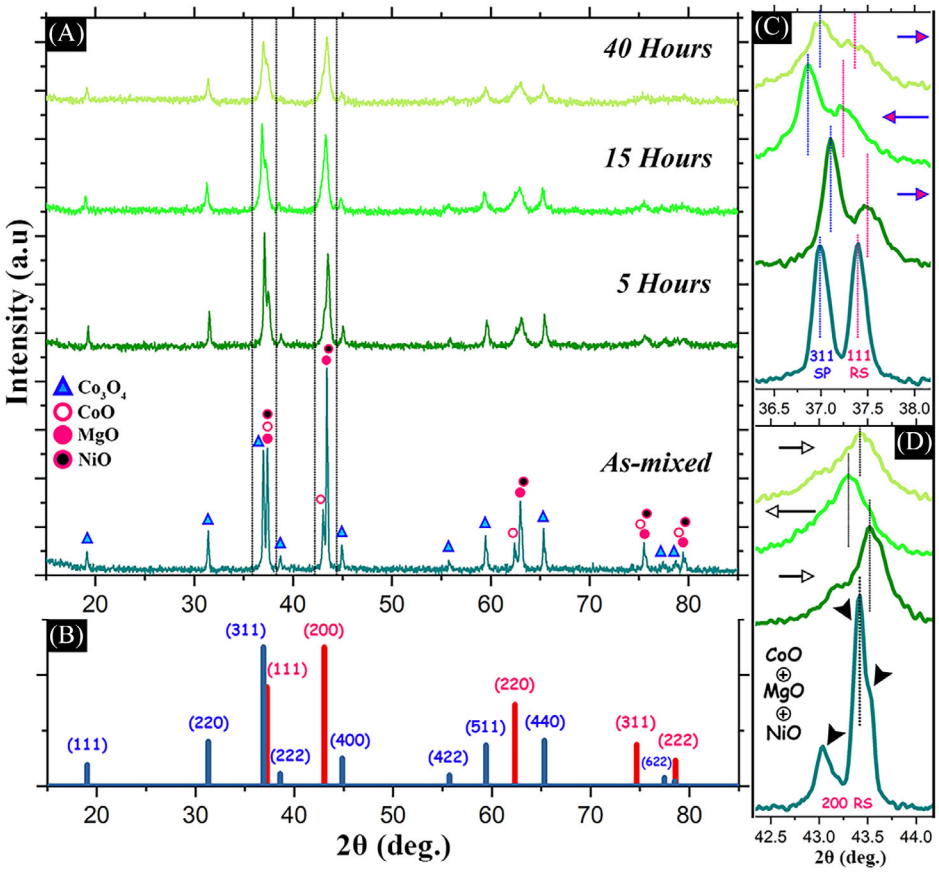

FIGURE 1 (A) X-ray diffraction (XRD) patterns of equimolar (CoMgNi)-oxide powder in the as-mixed condition and after 5, 15, and 40 h of ball milling. (B) Simulated XRD pattern of cubic rock salt (a ~4.2 Å) in red and cubic spinel (a ~8.1 Å) in blue, respectively. (C) Magnified view of 311 peak of cubic spinel and 111 peak of cubic rock salt in as-mixed condition and after 5, 15, and 40 h of ball milling. (D) Magnified view of the evolution of 200 peak of cubic rock salt phase in the as-mixed condition and after 5, 15, and 40 h of ball milling.

diffractometer with Cu-K_α ($\lambda = 1.54$ Å) and Co-K_α ($\lambda = 1.79$ Å) radiations. The diffractometer was operated at 40 kV accelerating voltage with 40 mA tube current. Both sides of the pellet were polished before examination. The sintered, quenched along with long-sintered, quenched as well as sintered, and quenched and aged multicomponent oxides were studied by a Tecnai G^2 T20 transmission electron microscope (TEM). For TEM observation, thin slices were obtained from the processed pellets by cutting them with a low-speed saw. A slice from the center of the pellet was crushed to powder. The crushed powder was suspended in ethanol and was ultrasonicated for 15 min before it was drop cast onto a carbon-coated copper grid of ~3 mm diameter. The XRD patterns were simulated by indigenously developed code and the structural models were developed by Vesta software.

3 | RESULTS

In the XRD pattern of the as-mixed equimolar mixture of Co(II, III)O, MgO, and NiO (Figure 1A), individual diffraction peaks of the precursor oxide phases could be easily discerned. The Co(II, III)O exists both in spinel and rock salt structures as evident from the XRD peaks marked by blue solid triangles and hollow open circles in red. MgO and NiO exist exclusively in rock salt structure as marked by red close circles and black filled close circles, respectively. The diffraction peaks of MgO and NiO are almost overlapping, which may be justified by the nearly similar lattice parameter and structure of the two oxides. The diffraction peaks of CoO with rock salt structure appears very close to the MgO and NiO diffraction peaks due to its similar structure, with a slightly larger lattice parameter. The experimentally observed diffraction patterns (Figure 1A) show excellent match with the simulated diffraction patterns (Figure 1B) of rock salt and spinel structures with a_{spinel} ~8.1 Å and $a_{\text{rock salt}}$ ~4.2 Å. The lattice parameters of MgO, NiO, and CoO were a ~4.21, ~4.15, and ~4.26 Å, respectively.

However, the lattice parameter of Co_3O_4 with spinel structure is a ~8.08 Å, which is almost double (lattice parameter ratio ~1.89) of the lattice parameter of the rock salt phase. The structural relationship between the rock

salt phase and the spinel phase will be discussed in terms of their nature of void filling in Section 4.

After 5 h of milling, the XRD peaks (Figure 1A) become broad due to the refinement of particle size and accumulation of strain in the lattice of the crystals. The peaks corresponding to the spinel phase continue to exist. There is a sharp reduction in the intensity of the peaks corresponding to the rock salt phase and the peaks corresponding to the CoO rock salt phase cannot be distinctly observed. It appears as a shoulder to the peaks corresponding to the NiO and MgO rock salt phases. It may be inferred that solid solutioning starts at the initial stages of milling. NiO and MgO acts as the host lattice in which CoO with rock salt structure starts getting incorporated. After 15 h of milling, the peaks (Figure 1A) are further broadened with reduction of intensity as strain continues to get accumulated with simultaneous reduction in the particle size. The peaks corresponding to the CoO phase with rock salt structure is completely merged with the peaks of the NiO and MgO phases. After 40 h of milling, only the spinel phase is observed distinctly and the rock salt phase is observed as a shoulder to the spinel phase. It may be inferred that after 40 h of milling, solid solution phase consisting of spinel and rock salt is formed in the initial stoichiometric mix of the elemental oxide powder.

A magnified view of the evolution of the (311) peak of the spinel phase and the (111) peak of the rock salt phase with the progress of milling is given in Figure 1C. As stated earlier, with the progress of milling, both the peaks are broadened and they start to merge with one another. The peak shifts and broadening may also be supported by a model that incorporates increasing amount of milling damage and defect formation. However, there is a slight rightward shift of the peaks after 5 h of milling, which becomes a net leftward shift after 15 h of milling and again a slight rightward shift after 40 h of milling. In order to rule out the effect of sample-height adjustment errors during characterization, the experiments have been performed multiple times. Change in d-spacing due to progressive solid solutioning is expected to be unidirectional in nature. In this case, switching of the shift direction may be attributed to the change in d-spacings and cell volume due to the accumulation of strain and vacancies in the lattice of the spinel and rock salt-based solid solution phases and the attempt of the phase mixture to optimize its vacancy concentration, composition, etc. Likewise, the magnified view of the (200) peak of the rock salt-based CoO, MgO, and NiO phases (Figure 1D) shows initiation of peak merger after 5 h of milling. After 15 h of milling, individual peaks of CoO, MgO, and NiO phases are not observed, indicating that the process of solid solution phase formation is mostly complete after 15 h of milling. However, along with the peak broadening, a slight rightward shift after 5 h of milling, a net leftward shift after 15 h of milling, and a slight rightward shift after 40 h of milling are observed. This may also be attributed to the accumulation of strain, increase in vacancy concentration in the rock salt-based solid solution phase, and the attempt of the phase to optimize its strain, vacancy concentration, and composition. It will be substantiated further in Section 4 in terms of ionic radii of the species and the structural similarity between rock salt and spinel phases.

XRD patterns of equimolar binary (MgNi)-oxide (in pink), (CoNi)-oxide (in blue), and ternary (CoMgNi)-oxide (in green) powder after sintering at 1473 K for 10 h are given in Figure 2A. In the binary (MgNi)-oxide, exclusively rock salt phase with a ~4.21 Å lattice parameter is observed. In the binary (CoNi)-oxide, cubic rock salt phase with a ~4.20 Å and a cubic spinel phase with a ~8.25 Å lattice parameters are observed. In the ternary (CoMgNi)-oxide, only cubic rock salt phase with a ~4.2 Å lattice parameter is observed. In the diffraction pattern of this ternary oxide, a small undulation corresponding to the (220) peak of a spinel phase is observed. However, the undulation is so small, it may not be used as a confirmation for the existence of the spinel phase. In order to further investigate the existence of the spinel phase, XRD patterns of the (CoMgNi)-oxide after sintering at 1473 K for 10 h in the pellet and powder form have been compared in Figure 2B(i and ii). In the XRD pattern of the pellet, a distinct (220) peak for spinel has been observed and other spinel peaks overlap with the peaks of the rock salt phase. It may be due to the low volume fraction of the spinel phase and its oriented growth with the rock salt phase. To further confirm the presence of the (220) peak of the spinel phase, repeated experiments with slower scan rates have been performed.

The normalized intensity plot of the experimental XRD patterns of the pellet and the crushed powder as shown in Figure 2B(i) are given in Figure 2B(ii). It is confirmed that the Compton inelastic background of the powder after crushing the sintered and quenched pellet is higher than the sintered and quenched pellet itself. Due to the high Compton background, in the XRD pattern of the crushed powder of the sintered and quenched pellet, the low intensity (220) peak of spinel may remain invisible. It is understandable that crushing of the pellet introduces strain that increases the Compton background scattering in the crushed powder. It may be inferred that low volume fraction of the spinel phase, its oriented growth with the rock salt phase, and concomitant increase in the Compton background scattering lead to the almost invisibility of the low intensity (220) peak of the spinel phase in the crushed powder. Similar changes in XRD patterns in entropy stabilized oxides and MCOs depending on processing conditions have been reported before.[32,33]

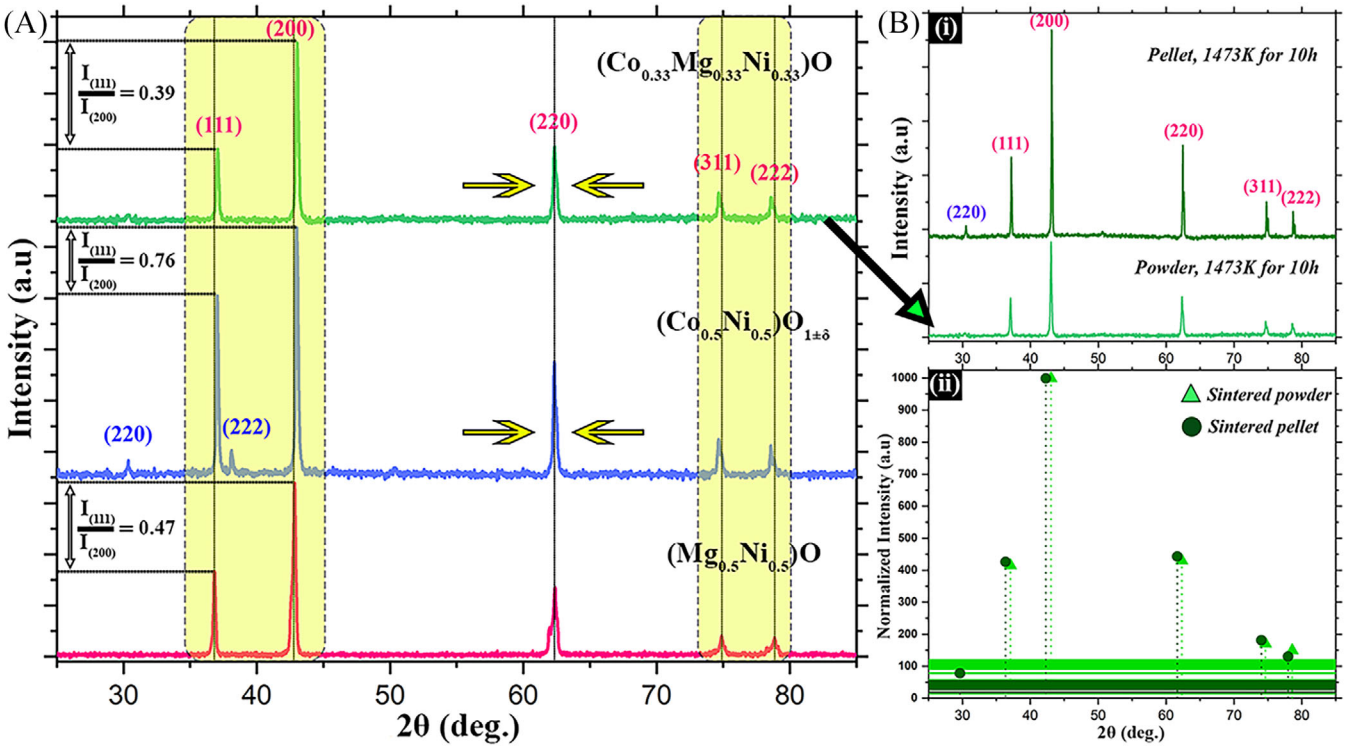

FIGURE 2 (A) X-ray diffraction (XRD) patterns of equimolar binary (MgNi)-oxide (in pink), (CoNi)-oxide (in blue), and ternary equimolar (CoMgNi)-oxide powder after sintering at 1473 K for 10 h followed by water quenching. (B) (i) XRD patterns of the equimolar ternary (CoMgNi)-oxide powder (light green) and pellet (dark green) after sintering at 1473 K for 10 h followed by water quenching. (ii) Normalized intensity plots from the experimental XRD patterns of the sintered and quenched (CoMgNi)-oxide in its powder and pellet form, in light and deep green, respectively. Compton modified scattering background is represented as bands with the respective colors.

TEM bright field (BF) image and electron diffraction patterns of (CoMgNi)-oxide after sintering at 1473 K for 10 h followed by water quenching are given in Figure 3A–D. The diffraction patterns from z = [011] (Figure 3A), z = [125] (Figure 3B), and z = [013] (Figure 3D) may be indexed to a cubic rock salt phase with a ~4.2 Å lattice parameter. In the corresponding BF image (Figure 3C), mottled contrast indicating the presence of residual strain is observed. It is noteworthy that the diffraction patterns from a cubic spinel phase with double the lattice parameter will appear to be very similar from similar zone axes as will be demonstrated later in this communication. However, in case of a spinel phase, some systematic extra spots should be observed, which are not present in the diffraction patterns.

As the selected area diffraction patterns are obtained from very localized regions, the signature of cubic spinel phase is absent. This corroborates the XRD results, where it has been stated that the spinel phase is present in a very small volume fraction. Around the diffraction spots, diffuse scattering is observed (Figure 3A,D) and in some of the diffraction spots, geometric shape evolution and splitting is observed (Figure 3A,B, inset). It will be discussed further in the subsequent sections. TEM CDF image (Figure 3E) and its corresponding BF pair (Figure 3E, inset) after aging the sintered and quenched sample at 723 K for 120 h shows extensive fringe contrast along with the mottled contrast. Magnified version of the BF image in Figure 3E (inset) is given in Figure 3F. The fringe contrast is clearly visible in the image. The fringes are marked with arrows in the image. The spacing between the fringes range from ~1.5 to 3.5 nm.

Electron diffraction patterns from the sintered and quenched sample and from the sintered, quenched, and aged sample along z = [001] are given in Figure 4. In the sintered, quenched, and aged sample, extensive splitting and arcing of spots with intensity modulation (Figure 4B) are observed. Different points in the diffracted arcs may be systematically joined together to bring out the symmetry shape corresponding to the fourfold [001] zone axis pattern of a cubic rock salt phase with a ~4.2 Å lattice parameter. Two such symmetry shapes by joining the extreme ends of the arcs are shown in the figure with colored dotted lines. It is observed that the symmetry shapes are rotated with respect to one another. Mutual rotation between two symmetry shapes formed by joining the extreme ends of the arcs is ~20°. It may be inferred that cubic rock salt domains with mutual rotation among them do exist in the aged

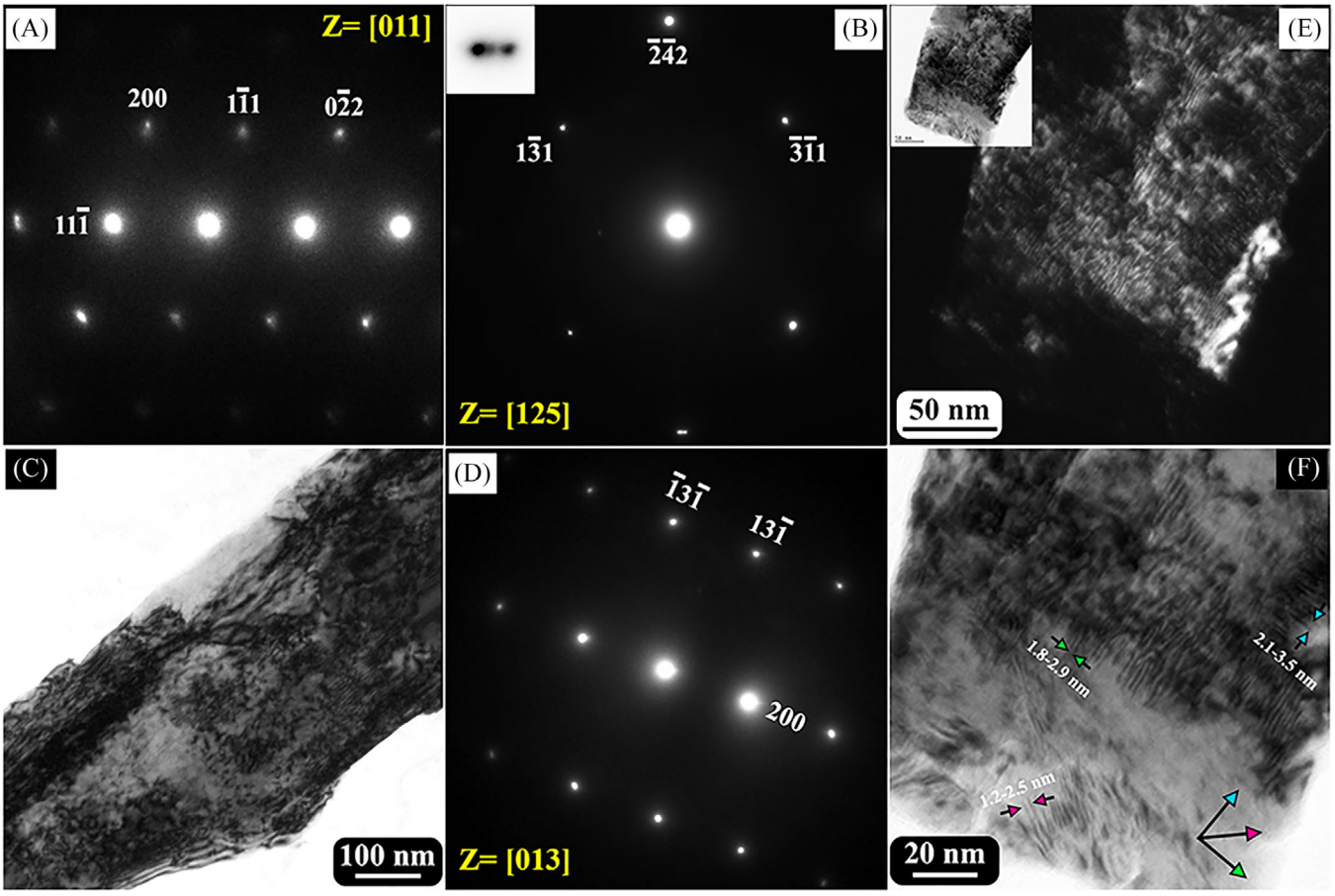

FIGURE 3 (A–D) Bright field (BF) image and selected area diffraction patterns along $z = [011]$, $z = [125]$, and $z = [013]$ zone axes from ternary equimolar (CoMgNi)-oxide after sintering at 1473 K for 10 h followed by water quenching. (E) Centered dark field (CDF) image and complementary BF image (inset) from the same ternary equimolar (CoMgNi)-oxide after sintering at 1473 K for 10 h followed by aging at 723 K for 120 h. (F) Magnified BF image of (E) showing multiply oriented fringes with ~1.5–3.5 nm spacing between them.

sample. It can be substantiated that the mutually rotated domains are developed during aging by comparing a similar diffraction pattern along $z = [001]$ from the sintered and quenched sample in Figure 4A. The diffraction pattern from the sintered and quenched sample (Figure 4A) along $z = [001]$ may be indexed to a cubic rock salt phase with a ~4.2 Å lattice parameter.

However, the arcing, splitting, and modulation of intensity are absent in the lower order spots. Minor arcing and spot splitting are observed in the higher order spots (circled in the diffraction pattern in Figure 4A). This necessarily means that the ternary, equimolar oxide tends to form a domain structure, which is strongly expressed when equilibrated at intermediate temperatures for longer time spans and subsequently more weakly expressed when equilibrated for lesser hours. It is further evidenced when the intensity distribution of the lower order spots perpendicular to the individual g-vectors is plotted in one dimension. Intensity distribution plots are given below the corresponding diffraction patterns in Figure 4(i–viii). The intensity distribution plots of the g-vectors for the sintered and quenched sample are mostly symmetric with a very minor skewness for the {2$\bar{2}$0} type spots (i–iv). In comparison to that, the intensity distribution plots of the diffraction spots for the sintered, quenched, and aged sample show multiple maxima with finite skewness (v–viii). Formation of mutually rotated domains in sintered, quenched, and aged sample manifest itself in the form of a fringe contrast in the BF and dark field (DF) images as observed in Figure 3E,F. Formation of such mutually rotated domains leading to a fringe contrast and tweed morphology has been observed after long hours of sintering and aging in (CaCoFeMgNi)-oxide[33] and (CoCuMgNiZn)-oxide,[32] respectively. It is understood that such tweed structures form in multicomponent oxide after long hours of sintering and/or aging in a bid to minimize its strain. It will be discussed further in Section 4.

Ternary equimolar (CoMgNi)-oxide has been partially substituted with Fe-ions, Mn-ions, and both Fe-ions and Mn-ions to form equimolar quaternary (CoFeMgNi)-oxide, (CoMgMnNi)-oxide, and equimolar quinary (CoFeMgMnNi)-oxide, respectively. XRD patterns of the

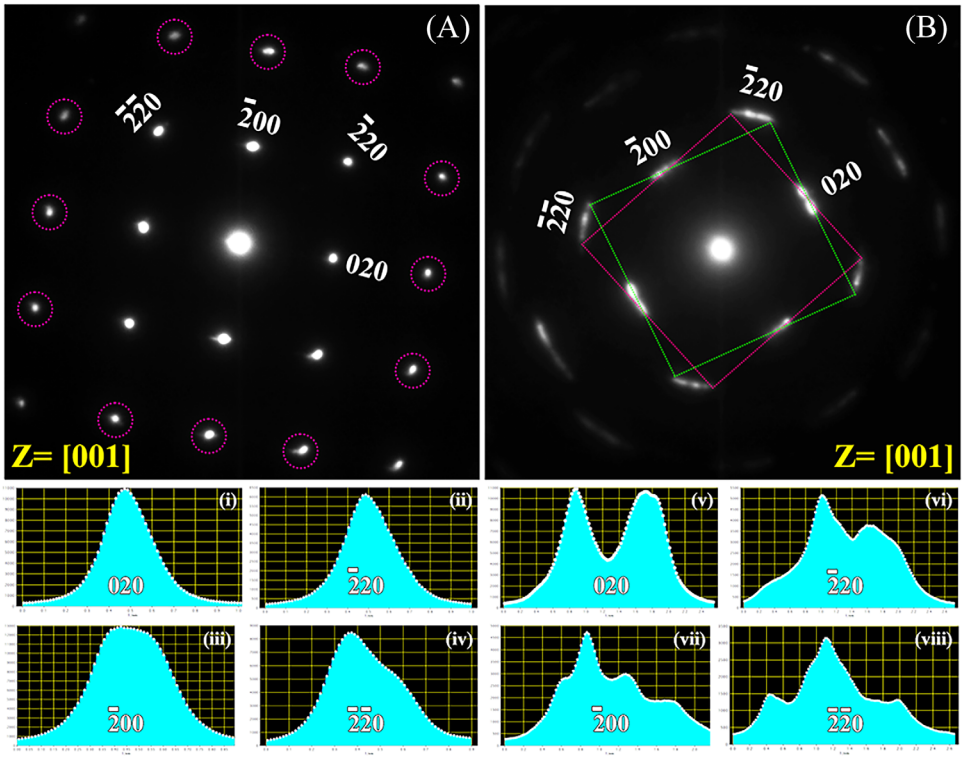

FIGURE 4 (A) Selected area electron diffraction pattern along $z = [001]$ zone axis of (CoMgNi)-oxide after sintering at 1473 K for 10 h followed by water quenching. Onset of splitting in the higher order spots (marked by dotted circles) is observed. (i–iv) Intensity distribution plots of {200} and {220} type spots are almost symmetrical. (B) Selected area electron diffraction pattern along $z = [001]$ zone axis of (CoMgNi)-oxide after sintering at 1473 K for 10 h, aging at 723 K for 120 h followed by water quenching. Diffraction spots are split and arced with modulation of intensity distribution. (v–viii) Intensity distribution plots of {200} and {220} type spots are not symmetrical with several maxima.

quaternary and quinary derivative oxides after sintering at 1473 K for 10 h followed by water quenching are given in Figure 5. As reported earlier, (CoMgNi)-oxide after sintering and quenching forms cubic rock salt phase with a ~4.2 Å lattice parameter. Upon systematic addition of Fe-ions, in the quaternary (CoFeMgNi)-oxide after sintering at 1473 K for 10 h followed by water quenching the cubic rock salt phase with a ~4.2 Å lattice parameter continues to exist.

However, the most intense (311) peak of a spinel phase with a ~8.4 Å lattice parameter appears. Upon systematic addition of Mn-ions, coexistence of two-phase mixture of a cubic rock salt with a ~4.2 Å lattice parameter and a cubic spinel with a ~8.4 Å lattice parameter is observed in the quaternary sintered and quenched (CoMgMnNi)-oxide. In the quinary (CoFeMgMnNi)-oxide, after sintering and quenching, predominantly a spinel phase with a ~8.38 Å lattice parameter is observed. It is worth mentioning that the diffraction peaks of a cubic rock salt phase with a ~4.22 Å (half the lattice parameter of the cubic spinel phase) lattice parameter will overlap with the diffraction peaks of the spinel phase. It is further evidenced by the presence of shoulders in the (222), (400), and (440) diffraction peaks

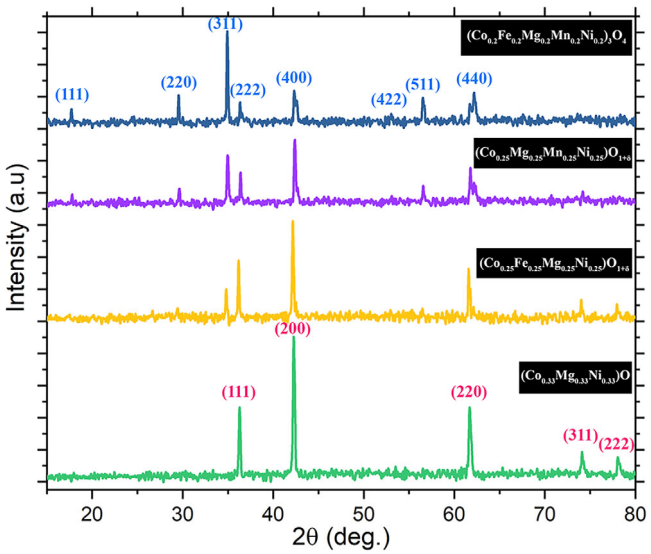

FIGURE 5 X-ray diffraction (XRD) patterns of (CoMgNi)-oxide with systematic addition of Fe-ions and Mn-ions after sintering at 1473 K for 10 h followed by water quenching. With systematic addition of Fe-ions and Mn-ions, the major phase in the equimolar multicomponent oxide changes from cubic rock salt phase to cubic spinel phase.

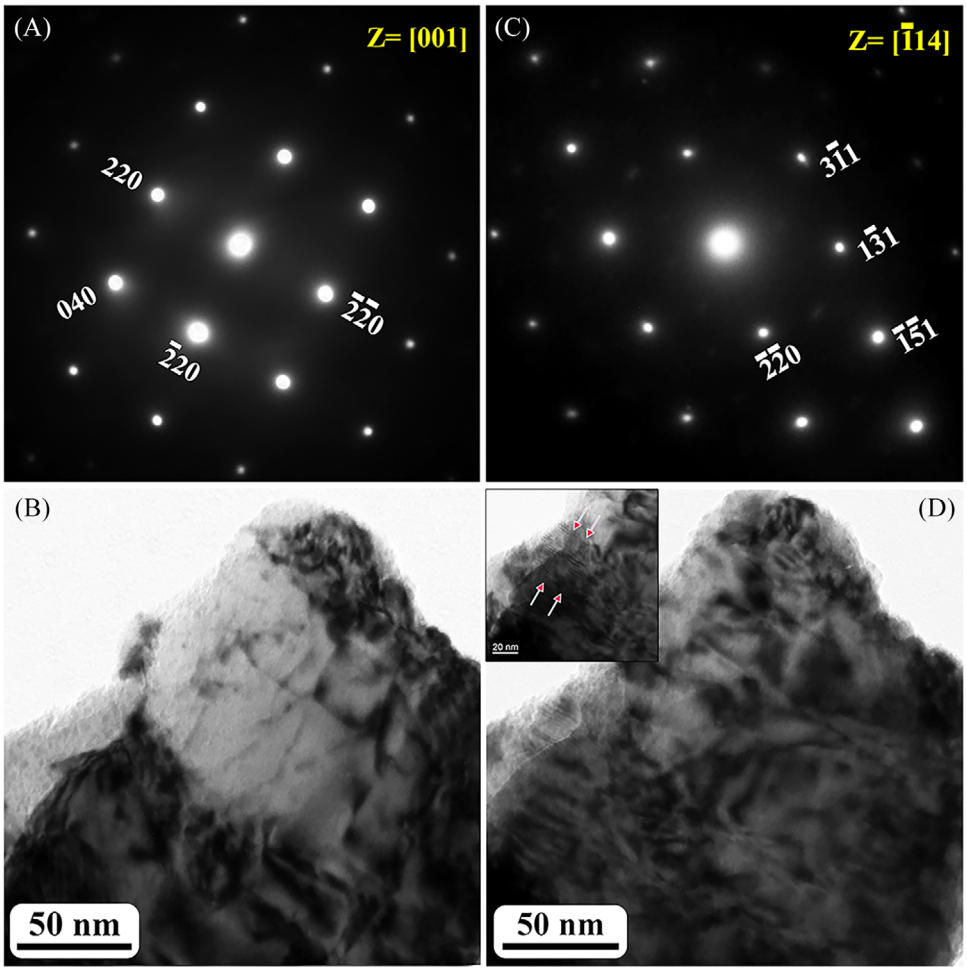

FIGURE 6 (A and C) Selected area electron diffraction patterns along $z = [001]$ and $z = [\bar{1}14]$ zone axes, respectively, and (B and D) bright field images of the multicomponent equimolar (CoFeMgMnNi)-oxide after sintering at 1473 K for 10 h followed by water quenching. Electron diffraction patterns are indexed to a cubic spinel phase (a ~8.38 Å). In the bright field images, mottled contrast with occasional fringe contrast (Figure 6D, inset) is observed.

of the spinel phase. It should be noted that, to the best of the knowledge of the authors, quinary multicomponent (CoFeMgMnNi)-oxide has not been reported before. It has been investigated further by electron diffraction after sintering for different lengths of time, which will be reported in the subsequent sections.

TEM BF images and corresponding electron diffraction patterns from (CoFeMgMnNi)-oxide after sintering at 1473 K for 10 h are given in Figure 6A–D. In the BF images, extensive mottled contrast is observed and the electron diffraction patterns along $z = [001]$ and $z = [\bar{1}14]$ may be indexed to a cubic spinel phase with a ~8.38 Å lattice parameter. It is noteworthy that in the BF image in Figure 6D, localized fringe contrast is observed. Magnified view of the fringe contrast is given in Figure 6D (inset). Existence of this linear Moire fringe contrast is indicative of two crystals with similar or nearly similar d-spacing are juxtaposed over one another with or without minor tilting. As it has been stated earlier, the structure of spinel and rock salt phase is quite similar. It may be the juxtaposition of a cubic rock salt phase over a cubic spinel phase. However, due to the paucity of the diffraction evidence, it may not be confirmed at this stage.

TEM BF images from different regions, corresponding electron diffraction patterns and their inverted versions with the indexing for (CoFeMgMnNi)-oxide after sintering at 1473 K for 100 h followed by water quenching are given in Figure 7A–F. In the BF image in Figure 7C, mottled and irregular fringe contrast is observed. Existence of such contrast may indicate presence of localized residual strain and structural modulation in the material. Corresponding electron diffraction pattern (Figure 7A) shows extensive spot splitting, arcing, and intensity modulation. The inverted version of the diffraction pattern is given in Figure 7B. The diffraction pattern may be indexed to a cubic spinel phase with a ~8.38 Å lattice parameter and a cubic rock salt phase with a ~ 4.22 Å lattice parameter.

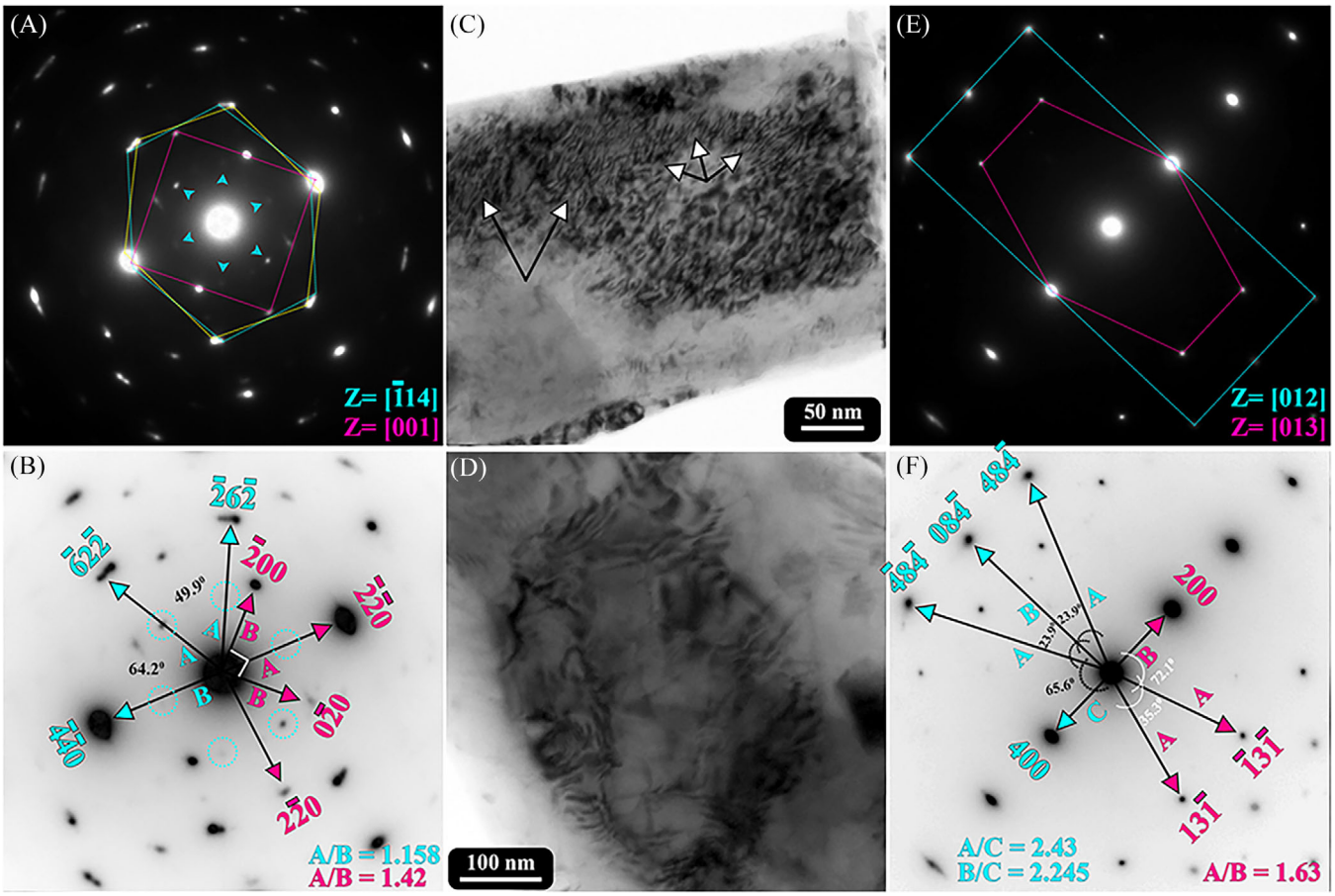

FIGURE 7 Selected area electron diffraction patterns (A-B) and bright field image (C) of (CoFeMgMnNi)-oxide after sintering at 1473 K for 100 h followed by water quenching. Diffraction pattern in (A) is indexed to a cubic spinel phase, $z = [\bar{1}14]$ zone axis along with a coexistent rock salt phase, $z = [001]$ zone axis. Indices of the diffraction spots, their angular relationships, and ratios of principal vectors are given in (B), which is inverted with respect to (A). Diffraction pattern in (E) is indexed to the same cubic spinel phase, $z = [012]$ zone axis along with the coexistent cubic rock salt phase, $z = [013]$ zone axis. Indices of the diffraction spots, their angular relationships, and the ratios of the principal vectors are given in (F), which is inverted with respect to (E). The corresponding bright field image is given in (D).

The diffraction vectors for the cubic spinel phase and the cubic rock salt phase along with their angular relationships and the ratios of the principal vectors are marked in Figure 7B in cyan and magenta colors, respectively. The diffraction pattern may be indexed to a $z = [\bar{1}14]$ zone axis pattern of a cubic spinel phase. It is noted that the first-order reflections in this zone axis are weak (marked by cyan arrows in Figure 7A and dotted circles in Figure 7B) and the second-order reflections are strong. The second-order reflections are strong as they are common to both the spinel and the rock salt phases. In addition, arcing, splitting, and intensity modulation in the second-order spots are observed. When the second-order spots are systematically joined together with dotted lines (Figure 7A), it clearly brings out the twofold symmetry shape corresponding to $z = [\bar{1}14]$ zone axis of a cubic spinel phase, which are rotated with respect to one another. This clearly indicates that the spinel phase forms structurally modulated domains, which are rotated with respect to one another. Formation of such rotated domains has been reported for quinary (CaCoFeMgNi)-oxide[33] and (CoCuMgNiZn)-oxide[32] after long hours of sintering or aging. It will be discussed further in Section 4. There are some additional diffraction spots in the diffraction pattern (Figure 7A) and its inverted version (Figure 7B). Those spots are marked in magenta along with the ratio of the principal vectors. The spots are joined together with magenta dotted lines (Figure 7B) that brings out a fourfold symmetry shape. The additional spots may be indexed to a cubic rock salt phase along $z = [001]$ zone axis with a ~4.22 Å lattice parameter. It is due to the simultaneous presence of a cubic spinel phase with a rock salt phase that intensity modulation is observed in the diffraction pattern. It is noteworthy that there is an orientation relationship between the rock salt phase and the spinel phase, which may be written as $[\bar{1}14]_{\text{spinel}} \| [001]_{\text{rock salt}}$ and $(440)_{\text{spinel}} \| (\bar{2}\bar{2}0)_{\text{rock salt}}$. BF image from a different region (Figure 7D) shows a domain like contrast in addition to the irregular fringe contrast.

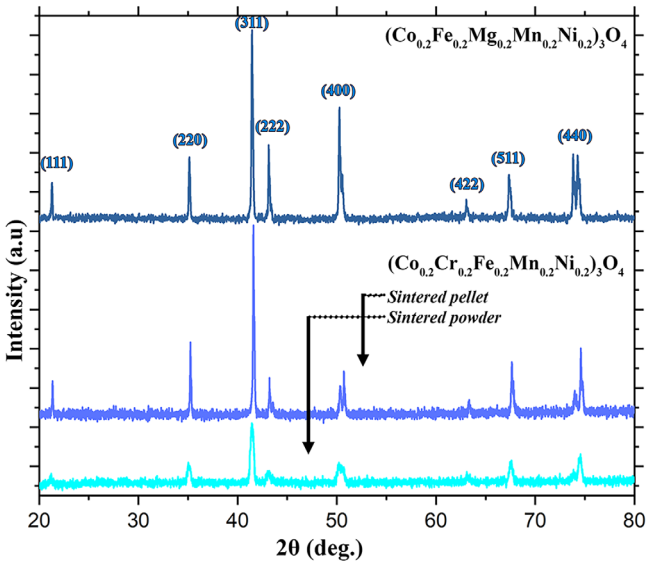

FIGURE 8 X-ray diffraction (XRD) patterns of (CoFeMgMnNi)-oxide and (CoCrFeMnNi)-oxide after sintering at 1473 K for 10 h followed by water quenching. In both of the multicomponent oxides, cubic spinel phase is observed to be the predominant phase with systematic peak splitting and shouldering.

The corresponding electron diffraction pattern and its inverted version are given in Figure 7E,F, respectively. In this diffraction pattern, modulation of intensity is observed and it may be indexed to $z = [012]$ zone axis of a cubic spinel phase and $z = [013]$ of a cubic rock salt phase. The spots corresponding to the spinel phase, rock salt phase, their principal vectors, and their ratios are marked in cyan and magenta, respectively. Similar orientation relationship is evident in this diffraction pattern. The orientation relationship is $[012]_{spinel} \| [013]_{rock\ salt}$ and $(400)_{spinel} \| (\bar{2}00)_{rock\ salt}$.

Effect of substitution of Cr-ions in place of Mg-ions in the quinary equimolar (CoFeMgMnNi)-oxide after sintering followed by quenching, which results into an equimolar quinary (CoCrFeMnNi)-oxide, has been studied by XRD and TEM. It is noteworthy that equimolar (CoCrFeMnNi)-oxide is the first ever reported single-phase spinel forming HEO.[9] It is also the oxide form of the first reported high-entropy Cantor alloy.[33,34], In the XRD pattern of the sintered and quenched (CoFeMgMnNi)-oxide (Figure 8), cubic spinel phase with a ~8.38 Å lattice parameter and cubic rock salt phase (a ~4.2 Å) in minor proportion are observed. In the XRD pattern of the (CoCrFeMnNi)-oxide after sintering at 1473 K for 10 h, cubic spinel phase with a ~8.36 Å lattice parameter is predominantly observed.

However, shoulders are observed in (222), (400), and (440) peaks, which can be directly indexed as the (111), (200), and (220) peaks of a cubic rock salt phase with half the lattice parameter. The XRD patterns of the same oxide after sintering and quenching, in pellet and powder form (Figure 8), have been compared and they do not show any significant difference except peak broadening and concomitant reduction in peak intensity. It may be inferred that in (CoCrFeMnNi)-oxide after sintering and quenching, cubic spinel phase forms predominantly. However, there might be a possibility of oriented growth of cubic rock phase with half the lattice parameter within the spinel phase.

TEM images and corresponding electron diffraction patterns of (CoCrFeMnNi)-oxide after sintering at 1473 K for 10 h followed by quenching are given in Figure 9A–F. In the electron diffraction pattern (Figure 9C) along $z = [001]$, clear fourfold symmetry of the zone axis is observed. The diffraction pattern may be indexed to a cubic spinel phase with a ~8.36 Å lattice parameter. It is noteworthy that the diffraction spots are diffused and a continuous streaking (marked by arrows) along {220} type vectors is observed. It necessarily indicates the presence of continuous structural modulation in the multicomponent oxide. In the BF image (Figure 9A), a fine scale modulation is observed. In the magnified version of the BF image, given in Figure 9D, coexistence of structural modulation along two perpendicular directions is observed.

The existence of such structural modulations leads to the formation of a domain morphology, which is ~5 nm × 5 nm in size. In the centered DF image (Figure 9B) with {220} spot under multibeam excitation, similar modulation is observed. The domains with alternate bright and dark contrasts are marked in Figure 9A,B with arrows. BF image of the same region with only <220> row of spots excited (Figure 9E) shows the modulation in only one direction perpendicular to the 220 reciprocal lattice vectors. The magnified version of the same region (Figure 9F) shows the modulation perpendicular to <220> direction with modulation wavelength of ~5 nm giving birth to a lamellar appearance. It may be inferred that the modulation develops in the spinel phase along <220> type directions. It will be discussed in detail in Section 4. The lattice parameters of the phase(s) from all the oxides have been represented in Table 1 for ease of understanding.

4 | DISCUSSION

Systematic synthesis followed by XRD and TEM experimentations of quinary equimolar (CoFeMgMnNi)-oxide, (CoCrFeMnNi)-oxide, and its binary, ternary, and quaternary derivative oxides establish a pattern in terms of evolution of cubic spinel and rock salt phases, their orientation relationship, and microstructural growth during sintering and aging heat treatments. Quinary multicomponent oxides and its derivatives are metastable in nature, which

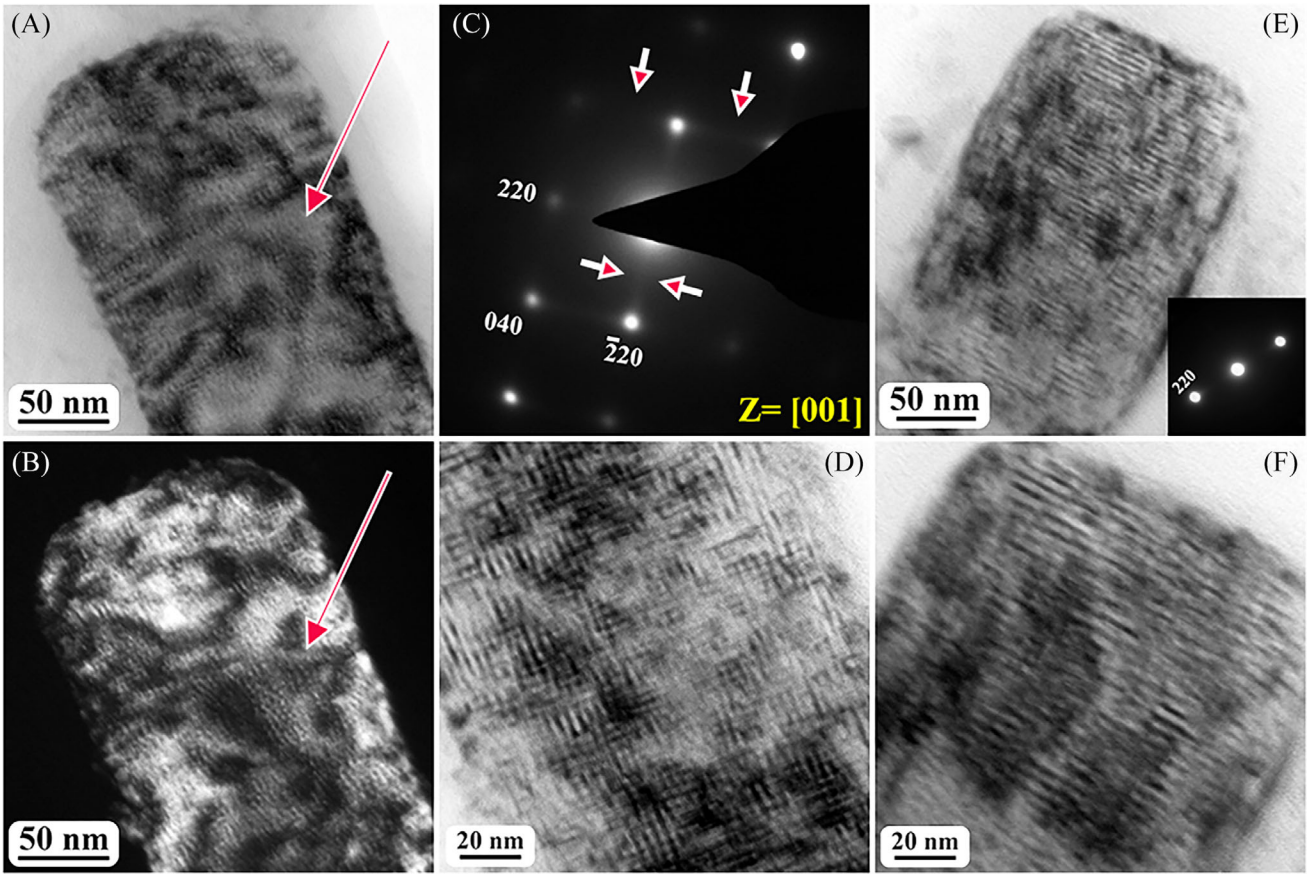

FIGURE 9 Bright field, centered dark field, and selected area electron diffraction patterns of (CoCrFeMnNi)-oxide after sintering at 1473 K for 10 h followed by water quenching. In the bright field image in (A) and corresponding centered dark field image in (B), modulation and formation of nanodomains are observed (marked with arrows). Corresponding diffraction pattern in (C) is indexed to a cubic spinel phase, z = [001] zone axis. Diffraction spots are diffused with streaking along mutually perpendicular <220> type directions (marked with arrows). In two-beam bright field image in (E) and (F) modulation along <220> direction is observed. Corresponding two beam diffraction pattern is given in the inset of (E). Cross-penetration of modulation leading to the formation of domains is shown in the high-magnification image in (D).

keep on changing its phase fraction, structural modulation, and microstructural growth. A bird's eye view of the fundamental nature of these equimolar multicomponent oxides is discussed in the following sections.

4.1 | Phase evolution and structural correlation between spinel and rock salt

Ternary equimolar mixture of Co(II, III)O, MgO, and NiO upon dry milling for 40 h results in a phase mixture of cubic spinel and rock salt phases. The lattice parameter of the resulting spinel phase is almost double of the rock salt phase. Initially, NiO and MgO oxide act as the host lattice for rock salt structure, in which CoO is incorporated. In the same line, Co_3O_4 phase with spinel structure acts as the host lattice for the spinel phase, in which Ni-ions and Mg-ions are incorporated. It is further observed that with the progress of milling and solid solution formation, strain-induced broadening of diffraction peaks takes place with a concomitant shift in its mean position (Figure 1). Shift in the peak position is not unidirectional. Shift in the peak position may directly be associated with the change in d-spacings, lattice parameter, and cell volume. It is understood that with the progress of milling, vacancy concentration in the lattice continue to increase. Continuous change in the vacancy concentration in the spinel and in the rock salt phase is one of the reasons behind the change in the d-spacings, lattice parameter, and the cell volume. As the spinel and the rock salt phases are associated through the vacancy concentration, the relative phase fraction of spinel and the rock salt phases changes leads to a shift in the mean position of the peak. In this connection, it is important to explain the structural correlation between the spinel phase and the rock salt phase. In both the phases, oxygen forms the FCC lattice; in case of the rock salt phase, all the octahedral voids are filled up with cations, and in case of the spinel phase,

TABLE 1 Equimolar multicomponent oxides, their heat-treatment conditions, phase(s), and lattice parameters.

	Multicomponent oxide	Heat treatment	Phase(s)	Lattice parameter (Å)
1.	$(Mg_{0.5}Ni_{0.5})$-oxide	1473 K, 10 h, WQ	Rock salt	4.21
2.	$(Co_{0.5}Ni_{0.5})$-oxide	1473 K, 10 h, WQ	Rock salt	4.2
			Spinel	8.25
3.	$(Co_{0.33}Mg_{0.33}Ni_{0.33})$-oxide	1473 K, 10 h, WQ	Rock salt	4.2
			Spinel	8.29
		1473 K, 10 h, WQ + 723 K, 120 h, WQ	Rock salt (with structural modulations)	4.18
4.	$(Co_{0.25}Fe_{0.25}Mg_{0.25}Ni_{0.25})$-oxide	1473 K, 10 h, WQ	Rock salt	4.2
			Spinel	8.4
5.	$(Co_{0.25}Mg_{0.25}Mn_{0.25}Ni_{0.25})$-oxide	1473 K, 10 h, WQ	Spinel	8.4
			Rock salt	4.2
6.	$(Co_{0.2}Fe_{0.2}Mg_{0.2}Mn_{0.2}Ni_{0.2})$-oxide	1473 K, 10 h, WQ	Spinel	8.38
		1473 K, 100 h, WQ	Spinel (with structural modulations)	8.38
			Rock salt	4.22
7.	$(Co_{0.2}Cr_{0.2}Fe_{0.2}Mn_{0.2}Ni_{0.2})$-oxide	1473 K, 10 h, WQ	Spinel (with structural modulations)	8.36

Abbreviation: WQ, water quenching.

half the octahedral voids are filled with cations. This explains that a spinel phase may transform to a rock salt when vacancy concentration is changed and vice versa, which is highly plausible during high-energy ball milling.

4.2 | Oriented growth of spinel, rock salt phases, and its interface structure

In the (CoMgNi)-oxide after sintering at 1473 K for 10 h, predominantly rock salt phase with a ~4.2 Å lattice parameter is observed. In the electron diffraction pattern of the rock salt phase, diffuseness in the primary diffraction spots and minor arcing associated with heavy splitting in the higher order spots is observed (Figures 3A–D and 4A,B). Diffuseness and split in the primary as well as higher order diffraction spots may be attributed to the residual strain in the rock salt crystal due to the presence of multiple cations in the phase.

Mottled contrast in the BF image (Figure 3C) confirms the presence of residual strain in the crystal. However, aging at 723 K for 120 h results in arcing in the diffraction spots (Figure 4B). It may be explained by the formation of structurally modulated domains in the rock salt phase and a continuous relative rotation between the domains. Structurally modulated domain formation and relative rotation between them takes place in order to reduce the lattice strain in the crystal. In the corresponding TEM images (Figure 3E,F), formation of irregular fringe contrast is observed. Inter-fringe spacing may directly be correlated with the stacking of domains with relative in-plane and out-of-plane rotations. Similar domain formation and relative rotation between them have been observed in (CaCoFeMgNi)-oxide and (CoCuMgNiZn)-oxide before.[32,33]

In quinary (CoFeMgMnNi)-oxide after sintering at 1473 K for 10 h, spinel phase forms predominantly. In the electron diffraction pattern of the spinel phase, similar diffuseness in the diffraction spots is observed (Figure 6A,C). When the quinary oxide is sintered for 100 h at 1473 K, modulation of intensity in the diffraction pattern and systematic appearance of extra spots are observed (Figure 7A,E) and it may be directly correlated to the oriented growth of a rock salt phase within the spinel phase with almost half the lattice parameter of the spinel phase. The interface diagram of the spinel phase with the rock salt phase has been presented schematically in Figure 10A,B. The interface, in all possibility, is semi-coherent. It is understood that such orientation relationship develops in a bid to reduce the interface strain through continuous reconstructive transformations at the interfaces. In a similar way, in the (CoCrFeMnNi)-oxide after sintering at 1473 K for 10 h, structurally modulated domains (Figure 9A–F) are observed with continuous diffuse streaking in the diffraction pattern along <220> type directions. Structural modulations in multicomponent oxides appear to be a common phenomenon in order to reduce strain in the crystal.[33,35] The structural and compositional modulations tend to grow with time, as has been reported before in (CoFeMn)-oxide[31] and multicomponent (CoFeGaMnZn)-oxide.[36]

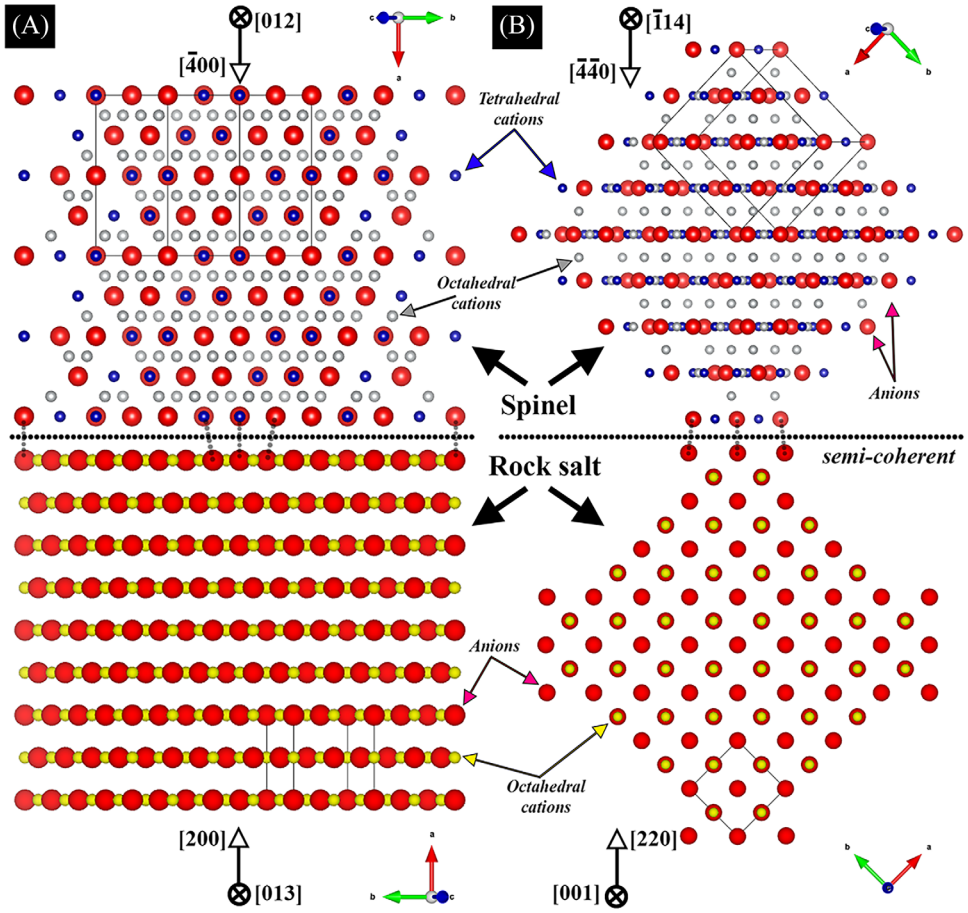

FIGURE 10 (A and B) Projected interface structure diagram between cubic spinel phase and cubic rock salt phase. Interface structure diagram has been developed based on the experimentally observed orientation relationship between the cubic spinel phase and the cubic rock salt phase. Interfaces are semi-coherent in nature.

4.3 | Stabilization through energy minimization

In the multicomponent quinary (CoFeMgMnNi)-oxide and (CoCrFeMnNi)-oxide, spinel phase forms after sintering. However, with prolonged sintering or aging, oriented growth of rock salt phase, development of structural modulation is clearly visible. It is also understood that oriented growth and structural modulation take place in order to minimize strain in the crystal. Acknowledging the kinetic unknowns, quinary multicomponent oxides are metastable in nature. With energy impetus from outside in the form of prolonged exposure at high/intermediate temperatures, these oxides try to reduce their energy through minimization of strain in the crystal, which manifests itself as domain formation, their relative rotation, coherent/semi-coherent interface formation, etc. Similar trend has been observed for (CaCoFeMgNi)-oxide and (CoCuMgNiZn)-oxide.[32,33] Multicomponent oxides are believed to be entropy stabilized. However, the authors have noted a complex interplay between entropy and strain energy that leads to the energy minimization. Gibbs free energy may be written as $\Delta G = \Delta H - T\Delta S$, where the symbols have their usual meaning. Furthermore, $\Delta H = \Delta U + P\Delta V$ for a constant pressure process. Combining both the equations, Gibbs free energy equation may be written as $\Delta G = \Delta U + P\Delta V - T\Delta S$. The term $P\Delta V$ represents mechanical energy associated with the transformation. In a multicomponent oxide, due to the presence of several cations in the lattice, configurational entropy is high, which in turn maximizes the negative contribution of the $T\Delta S$ term. However, maximizing the entropy comes with a cost of enhanced strain the lattice, which is reflected by the $P\Delta V$ term. In order to make the Gibbs free energy component optimally negative, the system tries to modulate itself compositionally and structurally that reduces the negative contribution of the entropy term. However, through structural and compositional modulations, it forms coherent/semi-coherent interface and reduces the lattice strain. That is how it reduces the positive contribution of the $P\Delta V$ term. It is a trade-off between the entropy and the strain energy that negatively minimizes the Gibbs free energy of the system. The authors would tend to believe that in multicomponent systems, it is not

only the entropy that determines the stability. It is a trade-off between entropy and strain energy that determines the stability of the system.[33]

5 | CONCLUSION

It may be concluded from the current work that high-energy ball milling in (CoMgNi)-oxide sets up a competition between rock salt and spinel phases, which is driven by the build-up of vacancies and its varying concentration in the phases, which keeps on changing with milling time. Equimolar ternary (CoMgNi)-oxide, previously believed to be the host structure for the entropic stabilization of quinary phase-pure (CoCuMgNiZn)-oxide with rock salt structure, coexists with small volume fraction of spinel phase. Furthermore, it is metastable with respect to intermediate temperature aging, and discrete lamellar colonies appear due to the formation of intergrown domain structure arising out of successive mutual in-plane and out-of-plane rotations. Systematic substitution of Mn-ions and Fe-ions in (CoMgNi)-oxide transforms the global average single-phase with rock salt structure to a global average single-phase with spinel structure in equimolar (CoFeMgMnNi)-oxide. Prolonged exposure to high temperature in (CoFeMgMnNi)-oxide leads to precipitation of a rock salt phase of half the lattice parameter, which develops definite orientation relationships with its parent spinel phase sharing semi-coherent interfaces. Structural modulation observed in sintered and quenched equimolar (CoCrFeMnNi)-oxide along <220> crystallographic directions was previously unanticipated. It also hints at local composition modulation-induced formation of nanometer-sized domains, which in turn brings out the shortcomings of the high entropy effect.

ACKNOWLEDGMENTS

The authors acknowledge financial support from the Department of Science & Technology, Government of India, through a FIST grant (TPN-32537) for the establishment and running of the IIT-(BHU) electron microscopy facility. Stimulating discussions with Prof. R.K. Mandal on several occasions is thankfully acknowledged.

ORCID

Joysurya Basu https://orcid.org/0000-0001-5155-2620

REFERENCES

1. Bian W, Li H, Zhao Z, Dou H, Cheng X, Wang X. Entropy stabilization effect and oxygen vacancy in spinel high-entropy oxide promoting sodium ion storage. Electrochim Acta. 2023;447:142157.
2. Zhai F, Zhu X, Zhang W, Cao G, Zhang H, Xing Y, et al. Insight of the evolution of structure and energy storage mechanism of $(FeCoNiCrMn)_3O_4$ spinel high entropy oxide in life-cycle span as lithium-ion battery anode. J Power Sources. 2024;603:234418.
3. Berardan D, Franger S, Dragoe D, Meena AK, Dragoe N. Colossal dielectric constant in high entropy oxides. Phys Status Solidi RRL. 2016;10:328–33.
4. Wu H, Lu Q, Li Y, Wang J, Li Y, Jiang R, et al. Rapid joule-heating synthesis for manufacturing high entropy oxides as efficient electrocatalysts. Nano Lett. 2022;22:6492–500.
5. Zhang J, Yan J, Calder S, Zheng Q, McGuire MA, Abernathy DL, et al. Long-range antiferromagnetic order in a rocksalt high entropy oxide. Chem Mater. 2019;31:3705–11.
6. Yang H, Chen Q, Zhu J, Jiang G, He L, Qiu N, et al. Selective construction of amorphous/crystalline heterostructure high entropy oxide for Li-ion batteries. J Alloys Comp. 2024;986:174140.
7. Segura MPJ, Takayama T, Berardan D, Hoser A, Reehuis M, Takagi H, et al. Long-range magnetic ordering in rocksalt-type high-entropy oxides. Appl Phys Lett. 2019;114:122401–5.
8. Rost CM, Sachet E, Borman T, Moballegh A, Dickey EC, Hou D, et al. Entropy-stabilized oxides. Nat Commun. 2015;6:9485.
9. Dabrowa J, Stygar M, Mikula A, Knapik A, Mroczka K, Tejchman W, et al. Synthesis and microstructure of the $(Co,Cr,Fe,Mn,Ni)_3O_4$ high entropy oxide characterized by spinel structure. Mater Lett. 2018;216:32–36.
10. Lin L, Wang K, Azmi R, Wang J, Sarkar A, Botros M, et al. Mechanochemical synthesis: route to novel rock-salt-structured high-entropy oxides and oxyfluorides. J Mater Sci. 2020;55:16879–89.
11. Musico BL, Gilbert D, Ward TZ, Page K, George E, Yan J, et al. The emergent field of high entropy oxides: design, prospects, challenges and opportunities for tailoring material properties. APL Mater. 2020;8:040912.
12. Clement RJ, Lun Z, Ceder G. Cation-disordered rocksalt transition metal oxides and oxyfluorides for high-energy lithium-ion cathodes. Energy Environ Sci. 2020;13:345–73.
13. Rost CM, Schmuckler DL, Bumgardner C, Hoque MSB, Diercks DR, Gaskins JT, et al. On the thermal and mechanical properties of $Mg_{0.2}Co_{0.2}Ni_{0.2}Cu_{0.2}Zn_{0.2}O$ across the high-entropy to entropy-stabilized transition. APL Mater. 2022;10:121108.
14. Hong W, Chen F, Shen Q, Han YH, Fahrenholtz WG, Zhang L. Microstructural evolution and mechanical properties of (Mg,Co,Ni,Cu,Zn)O high-entropy ceramics. J Am Ceram Soc. 2019;102:2228–37.
15. Lu J, Lee KS. Spinel cathodes for advanced lithium ion batteries: a review of challenges and recent progress. Mater Technol. 2016;31(11):1–14.
16. Usharani NJ, Shringi R, Sanghavi H, Subramanian S, Bhattacharya SS. Role of size, alio-/multi-valency and non-stoichiometry in the synthesis of phase-pure high entropy oxide (Co,Cu,Mg,Ni,Na,Zn)O. Dalton Trans. 2020;49:7123.
17. Yang H, He L, Yang Z, Chen Q, Jiang G, Zhu J, et al. Design optimization of spinel-rocksalt intergrown high entropy oxide structure for enhanced electrochemical properties. J Alloys Comp. 2023;968:172135.
18. Dupuy AD, Chellali MR, Hahn H, Schoenung JM. Nucleation and growth behaviour of multicomponent secondary phases in entropy-stabilized oxides. J Mater Res. 2023;38:198–214.

19. Dupuy AD, Chiu IT, Shafer P, Arenholz E, Takamura Y, Schoenung JM. Hidden transformations in entropy-stabilized oxides. J Eur Ceram Soc. 2021;41:6660–69.
20. Rak Z, Maria JP, Brenner DW. Evidence for Jahn–Teller compression in the (Mg,Co,Ni,Cu,Zn)O entropy-stabilized oxide: a DFT study. Mater Lett. 2018;217:300–303.
21. Frachhia M, Coduri M, Manzoli M, Ghigna P, Tamburini UA. Is configurational entropy the main stabilizing term in rock-salt $Mg_{0.2}Co_{0.2}Ni_{0.2}Cu_{0.2}Zn_{0.2}$ high entropy oxide? Nat Commun. 2022;13:2977.
22. Anand G, Wynn AP, Handley CM, Freeman CL. Phase stability and distortion in high-entropy oxides. Acta Mater. 2018;146:119–25.
23. Grzesik Z, Smola G, Stygar M, Dabrowa J, Zajusz M, Mroczka K, et al. Defect structure and transport properties in (Co,Cu,Mg,Ni,Zn)O high entropy oxide. J Eur Ceram Soc. 2019;39:4292–98.
24. Baek J, Hossain MD, Mukherjee P, Lee J, Winther KT, Leem J, et al. Synergistic effects of mixing and strain in high entropy spinel oxides for oxygen evolution reaction. Nat Commun. 2023;14:5936.
25. Almishal SSI, Miao L, Tan Y, Kotsonis GN, Sivak JT, Alem N, et al. J Am Ceram Soc. 2025;108:20223.
26. Navrotsky A, Kleppa OJ. The thermodynamics of cation distributions in simple spinels. J Inorg Nucl Chem. 1967;29:2701–14.
27. Horibe Y, Takeyama S, Mori S. Large-scale phase separation with nano-twin domains in magnetite spinel $(Co,Fe,Mn)_3O_4$. AIP Conf Proc. 2016;1763:050005.
28. Davies PK, Akaogi M. Phase intergrowths in spinelloids. Nature. 1983;305:788–90.
29. Sickafus KE, Wills JM, Grimes NW. Spinel compounds: structure and property relations. J Am Ceram Soc. 1999;82:3279–92.
30. Singh A, Yasui S, Pal AS, Bendersky LA, Takeuchi I, Mandal RK, et al. Structure and interfaces of compositionally graded $Li(Ni,Mn)_xO_y$ cathodes on (111) Nb-doped $SrTiO_3$. Philos Mag. 2022;102:1547–79.
31. Pal AS, Das AKL, Gururaj K, Sadhasivam M, Knowles KM, Ahmad MI, et al. Nanoarchitectonics of self-assembled chessboard-like structures by recurrent phase separation and coalescence of nano domains in CoFeMn oxide. Acta Mater. 2023;242:118423.
32. Mukherjee S, Mukhopadhyay NK, Basu J. Local composition modulation and oriented inter-growth induced strain minimization in entropy stabilized (CoCuMgNiZn) oxide (Communicated).
33. Mukherjee S, Mukhopadhyay NK, Basu J. Composition modulation, strain minimization and oriented growth of phases in equimolar (CaCoFeMgNi) multicomponent oxide. Acta Mater. 2025;285:120621.
34. Cantor B, Chang ITH, Knight P, Vincent AJB. Microstructural development in equiatomic multicomponent alloys. Mater Sci Eng A. 2004;375–377:213–18.
35. Berardan D, Meena AK, Franger S, Herrero C, Dragoe N. Controlled Jahn–Teller distortion in (MgCoNiCuZn)O-based high entropy oxides. J Alloys Comp. 2017;704:693–700.
36. Pal AS, Das AKL, Singh A, Knowles KM, Ahmad MI, Basu J. Evolution of a self-assembled chessboard nanostructure spinel in a CoFeGaMnZn multicomponent oxide. Philos Mag. 2022;102(12):1121–35.

How to cite this article: Mukherjee S, Mukhopadhyay NK, Basu J. Structural modulation, oriented growth of rock salt, and spinel in (Co(Cr/Mg)FeMnNi) multicomponent oxide and derivatives. J Am Ceram Soc. 2025;108:e20619. https://doi.org/10.1111/jace.20619